

Spherical Infall in G10.6-0.4: Accretion Through an Ultracompact HII Region

Peter K. Sollins¹, Qizhou Zhang¹, Eric Keto¹, Paul T. P Ho¹

ABSTRACT

We present high resolution ($0.''12 \times 0.''079$) observations of the ultracompact HII region G10.6-0.4 in 23 GHz radio continuum and the $\text{NH}_3(3,3)$ line. Our data show that the infall in the molecular material is largely spherical, and does not flatten into a molecular disk at radii as small as 0.03 pc. The spherical infall in the molecular gas matches in location and velocity the infall seen in the ionized gas. We use a non-detection to place a stringent upper limit on the mass of an expanding molecular shell associated with pressure driven expansion of the HII region. These data support a scenario in which the molecular accretion flow passes through an ionization front and becomes an ionized accretion flow onto one or more main sequence stars, not the classical pressure-driven expansion scenario. In the continuum emission we see evidence for externally ionized clumps of molecular gas, and cavities evacuated by an outflow from the central source.

Subject headings: stars: formation — ISM: individual (G10.6-0.4) — HII regions — accretion

1. Introduction

The ultracompact (UC) HII region G10.6-0.4, at a distance of 6.0 kpc (Downes et al. 1980), is the brightest member of a complex of variously compact HII regions (Wood & Churchwell 1989b) in an area of active star formation. The associated IRAS point source, IRAS 18075-1956, has a luminosity of $9.2 \times 10^5 L_\odot$ (Casoli et al. 1986) and has colors that meet the criteria of Wood & Churchwell (1989a) for an UCHII region. G10.6 is known to be embedded in a hot molecular core (HMC) (Braz & Epchtein 1983; Ho & Haschick 1986; Plume et al. 1992). The core is thought to contain at least $1200 M_\odot$ of gas within a radius of 0.2 pc, based on an analysis of a variety of dust continuum measurements (Mueller et al.

¹Harvard-Smithsonian Center for Astrophysics, 60 Garden Street, Cambridge, MA, 02138, psollins@cfa.harvard.edu

2002), and at least $3300 M_{\odot}$ of gas within 1.1 pc based on $C^{18}O$ and $C^{17}O$ measurements (Hofner et al. 2000). Previous studies of the inversion lines of NH_3 have determined that the molecular core is rotating and collapsing inward toward the UCHII region (Ho & Haschick 1986; Keto et al. 1987b, 1988; Keto 1990). In these studies, using the $NH_3(1,1)$ and $NH_3(3,3)$ lines, rotation is seen at size scales from 1 pc down to 0.08 pc, and infall is detected in the form of red-shifted absorption seen against the continuum source. CH_3OH and H_2O masers are seen distributed linearly in plane of the rotation (Walsh et al. 1998; Hofner & Churchwell 1996), while OH masers seem to be distributed along the axis of rotation (Argon et al. 2000). In $C^{18}O$ ($J = 1 \rightarrow 0$), Ho et al. (1994) see $10^3 M_{\odot}$ of dense ($n \sim 10^6 \text{cm}^{-3}$), rotating gas in a flattened (0.3×0.1 pc) disk-like structure. At the highest resolution achieved in earlier work, infall and rotation in the molecular gas were seen simultaneously in absorption, showing that the molecular gas was spiraling inward on size scales comparable to the size of the UCHII region. Our new observations resolve the UCHII region and show clearly that the molecular gas is infalling mostly spherically toward the UCHII region, with only slow rotation and little flattening in the plane of rotation.

Recent observations of the ionized gas within the UCHII region showed that the ionized gas is also spiraling inward toward the stars at the center of the UCHII region (Keto 2002a). Subsequent theoretical work showed that in small HII regions, the gravitational effect of the central star(s) can overcome the thermal pressure of the ionized gas causing the molecular accretion flow to pass through the HII region boundary and continue inward as an ionized accretion flow (Keto 2002b). In this model, the HII region boundary exists as a standing R-type ionization front within a continuous accretion flow. These results differ from classical treatments of the pressure driven expansion of HII regions, which predict outward motion of the ionized gas as soon as the HII region is formed (Strömgren 1939; Spitzer 1978). In the classical model for pressure driven expansion, the HII region boundary, after a very short phase as a moving R-type front, will develop a characteristic double front structure composed of an isothermal shock followed by a moving D-type ionization front. In this model, as the HII region expands, most of the displaced molecular material remains between the shock and the ionization front as a dense outward moving shell, which snow-plows ahead of the HII region. In the alternative model of Keto (2002b), however, the accretion flow passes through a standing R-type ionization front at the HII region boundary and continues toward the star(s) as an ionized flow. In that case there will be no swept-up, dense molecular layer at the boundary, and all the molecular gas will be moving inward. Ionized accretion flows represent a fundamentally different mode of accretion than that seen in low-mass star formation. In the ionized accretion flow scenario a main sequence star accretes gas which was once part of a molecular accretion flow, but has been photo-ionized as it approaches the star. G10.6 contains the first example of evidence for a massive accretion flow continuing

through an ionization front. Our new observations constitute a stringent non-detection of any outward moving molecular layer thus contradicting the pressure driven expansion model (see Section 3.3).

2. Observations

We observed the UCHII region G10.6 with the NRAO Very Large Array (VLA)¹ on February 1, 2002, with the phase center at $\alpha(2000) = 18^{\text{h}}10^{\text{m}}28^{\text{s}}.68$, $\delta(2000) = -19^{\circ}55'49''.07$. We observed the (3,3) inversion line of NH_3 at 23.870130 GHz with 63 spectral channels of width 48.828 kHz (0.61 km s^{-1}) for a total bandwidth of 3.125 MHz (38.7 km s^{-1}) centered on $v_{\text{lsr}} = 10 \text{ km s}^{-1}$, and 1.3 cm continuum with a bandwidth of 15.6 MHz. The array was in the A-configuration, yielding a uniform-weighted synthesized beam of width $0.''12 \times 0.''072$ for a physical resolution of $0.0034 \times 0.0021 \text{ pc}$ or $700 \times 430 \text{ AU}$.

We observed the quasars 3C286, 3C273 and 1733-130 for flux, bandpass and phase calibration respectively. Self-calibration of the source amplitudes and phases resulted in a noise level of 0.18 (0.14) mJy beam⁻¹ in the uniform (natural) weighted continuum map, and 1.9 (1.5) mJy beam⁻¹ in each uniform (natural) weighted channel map, about 3 times the thermal noise limit. Expressed as a temperature, our sensitivity in a natural weighted continuum map is about 25 K and in a natural weighted channel map is about 280 K. The physical temperature of the molecular gas around G10.6 is estimated to be only 110 K at the ionization front (Keto 1990). Thus, none of the molecular gas is detectable in thermal line emission in channel maps at the 3σ level. But since the continuum has a peak brightness temperature of 6900 K, the line absorption can be detected at roughly 25σ in a single channel. The quality of the self-calibration solutions and improvements in the K-band receiver system at the VLA have resulted in 25 times better sensitivity in our $\text{NH}_3(3,3)$ channel maps than in the previous best existing $\text{NH}_3(3,3)$ data for this source (Keto et al. 1988), with 3 times better spatial resolution and 2 times better velocity resolution.

¹The National Radio Astronomy Observatory is a facility of the National Science Foundation operated under cooperative agreement by Associated Universities, Inc.

3. Results

3.1. The Structure of the HII Region

Figure 1 shows the 23 GHz continuum map in both panels. The color-scale in the left panel is stretched to emphasize the structure in the weaker emission while the right panel is scaled to show clearly the structure in the strongest emission. Four features in particular, marked A1-A6, B1-B5, C, and D in Figure 1, are worth noting.

First, to the east of the main UCHII region, there are six arc shaped continuum sources marked A1 through A6 in Figure 1. Several of these are arcuate, and convex, pointing back toward the central UCHII region. All except for A1 are brightest on their western edges as if they are externally ionized by photons from the HII region or mechanically by a wind. Arcs A2-A5 show line absorption (see Figure 2) suggesting that they are embedded inside the HMC. Because A1 is also bright enough to show detectable absorption, but does not, A1 must either be in front of the densest gas, or the gas toward A1 might have lower column density or might not be warm enough to populate the (3,3) state. The upper limit on the optical depth of the $\text{NH}_3(3,3)$ main hyperfine line toward A1 is $\tau_\nu < 0.6$. By contrast, toward the continuum peak, we detect an optical depth of the main hyperfine line in excess of 65.

Second, there are larger scale linear structures extending to the south and northeast from the main UCHII region marked B1 and B2 in Figure 1. In the right panel of Figure 1 there are smaller scale linear features marked B3, B4 and B5. One can envision a wide angle outflow with an evacuated cavity whose edges are defined by B1, B3 and B4 on the southwest and by B2 and B5 on the northeast, parallel to the axis of rotation of the molecular gas, which is about 40 degrees east of north (Keto et al. 1987a, 1988). The outflow would fill the “V” shape on the northeast edge of the UCHII region. There is no $\text{NH}_3(3,3)$ absorption above the sensitivity limit of optical depth 0.3 toward source B1. We suggest that B1 defines the edge of the cavity evacuated by the southwest side of the outflow, protruding toward the observer out of the densest molecular gas. Ongoing observations in the $\text{H66}\alpha$ line in this region have measured the motion of ionized gas in the cavities, with the southwest side (B1, B3, B4) moving toward the observer, and the northwest side (B2, B5) moving away. The general shape of the brightest continuum emission is extended perpendicular to the rotation axis with an aspect ratio of about 2, which is consistent with there being an ionized disk perpendicular to the proposed outflow along the rotation axis.

Third, the slightly resolved, almost circular peak just to the northwest of the main HII region, marked C in Figure 1, may be a separate “hyper-compact” HII region. Because of its regular shape, it seems unlikely that the ionization is caused by UV photons leaking out of the central HII region. If this is a distinct, extremely compact HII region, its radius, $\sim 0''.08$

or about 500 AU, is consistent with gravitational trapping of the ionized gas by $100 M_{\odot}$ of stars (Keto 2002b).

Fourth, while there are some sharp edges in the continuum emission, for instance, in sources B1 and B2, the edges of the main UCHII region itself are quite gradual, even “frothy”. This froth is marked D in Figure 1. This frothy edge structure is present all around the UCHII region except in the regions which we propose to be the evacuated outflow cavity. So in a scheme in which accretion is going on through a flattened structure and outflow is going on along the rotation axis, we can associate the froth with irregularities specifically in that part of the ionization front through which accretion is taking place. The irregular structures could be related to varying density in the gas crossing the ionization front, or photo-ionization of a very clumpy circumstellar environment. Several possible ionization front instabilities are discussed in Keto & Ho (1989), but because the continuum in this part of the map is weak we do not have line data to help us distinguish between different possibilities.

The much sharper ionization fronts associated with B1 and B2 could be due to the much higher velocities in the outflow and an evacuated environment in the direction of the outflow. Finally the isolated nature of A2-A6, with no intervening ionized structures to the central source, also suggests a clumpy circumstellar environment. To be consistent with the frothy structure seen towards the central region, the size-scale and separation of clumps must increase away from the center. Future work, in which we will map the radio continuum at high resolution in a variety of frequencies, will allow us to carefully determine the spectral energy distribution for comparison to models, such as those of Ignace & Churchwell (2004), of clumpy UCHII regions.

3.2. Resolving the Infall Motions

Our absorption line data clearly show that infall dominates the kinematics of the molecular gas. Figure 2 is a map of the first moment (that is the flux-weighted average velocity) of the main hyperfine component of the $\text{NH}_3(3,3)$ absorption line. While previous work done at lower angular resolution relied on P-V diagrams to determine the velocity of the gas as a function of position (Keto et al. 1987a, 1988), our higher resolution data allow us to map the velocity of the line at every position in the two dimensional map, not just along selected one dimensional cuts. The velocity of the absorbing gas ranges from $v_{\text{lsr}} = +3.5 \text{ km s}^{-1}$ shown as white in Figure 2, to $v_{\text{lsr}} = -2.5 \text{ km s}^{-1}$ shown as purple. The velocity of the ambient gas, as determined from widespread emission seen at lower resolution and subsequent radiative transfer modeling is $v_{\text{lsr}} = -3.0 \text{ km s}^{-1}$ (Ho & Haschick 1986; Keto 1990). Thus the white points in Figure 2, i.e. the most red-shifted points, show the peak of the infall. Moving

away from that peak position in any direction, the infall velocity decreases, forming concentric rings of red, orange, and yellow in Figure 2. The smooth, circular pattern of radially decreasing red-shift is indicative of spherical infall, in which the line-of-sight infall velocity gets projected out as one moves away from the center of infall (Ho & Haschick 1986). The velocity pattern is dominated by this “bulls-eye” pattern created by the spherical infall.

There is also evidence in Figure 2 of the rotation that was seen at larger radii, out to 1 pc (Ho & Haschick 1986). Earlier work has shown that the rotation axis runs from southwest to northeast, with the rotating gas coming toward the observer in the southeast and going away from the observer in the northwest (Ho & Haschick 1986; Ho et al. 1994). The rotation is apparent in Figure 2 only as a perturbation to the “bulls-eye” pattern of spherical infall. The effect of the rotation is to shift the apparent center of infall along the plane of rotation, toward the northwest, where the rotational velocity is away from the observer along the line of sight. Although the rotation is evident in Figure 2, the circular velocity at a radius of 0.03 pc is 2 km s^{-1} , which is less than the infall velocity. The molecular gas is therefore spiraling inward to the UCHII region without first settling into a disk.

Despite the rotation seen at larger radii, we see no evidence for the molecular gas settling into a disk at a radius of 0.03 pc. The optical depth of the absorbing gas, calculated from the ratio of the absorption in the main and satellite hyperfine components, shows an overall radial drop-off from a peak in the center and a slight trend toward higher optical depths in the plane of rotation, suggesting a somewhat flattened, but mostly spherical density structure as opposed to a geometrically thin molecular disk. By contrast, if the molecular accretion flow were geometrically thin in the plane of rotation of the core, as in, for instance, a rotationally supported disk, then any inclination of the molecular disk to the line of sight would result in high optical depth on one side of the HII region and much lower optical depth on the other side. This optical depth pattern is not detected. The more spherical density structure is consistent with the mainly spherical velocity structure of the flow. While rotation dominates at larger radii as shown by Ho & Haschick (1986); Keto et al. (1988); Ho et al. (1994), our data show that at a radius of 0.03 pc, rotation does not dominate. No disk is formed at that radius. While the rotational velocities increase inward (Keto et al. 1988), the infall increases inward more quickly, and dominates as the gas crosses the UCHII region boundary. The molecular gas apparently spirals into the UCHII region without first settling into a molecular disk. This certainly does not preclude the possibility of an ionized disk inside the UCHII region.

Most of the line absorption must take place very close to the UCHII region. Because we see the effects of projection in both the spherical infall and the rotation components of the velocity structure, the geometry requires that the absorbing gas be immediately outside

the HII region and wrap closely around the continuum backlight. If the absorbing gas were not right up against the continuum source, the radial motions would not show significant projection effects away from the center of infall, and the velocity would not return to the ambient velocity at the edge of the absorption, as it does. For this reason, we can associate the infall and rotation velocities seen in the absorbing gas with the radius of the UCHII region. We also note that the optical depth falls off by a factor of ~ 100 from the center of the UCHII region to the continuum sources A1-A6, which is consistent with the centrally condensed and centrally heated molecular core model of Keto (1990). A strongly centrally condensed core naturally locates most of the absorbing material, and therefore most of the absorption, physically close to the continuum source.

An important connection can be made between the infall we see in the molecular gas just outside the UCHII region, and the motions of ionized gas inside the UCHII region. Keto (2002a) found that the H66 α radio recombination line showed infall motions in the ionized gas inside the UCHII region. Figure 2 of that paper is a map of the first moment of the H66 α line at 1'' resolution. Comparing Keto (2002a) and our Figure 2 shows that the H66 α and NH₃(3,3) lines have the same peak infall velocity at the same position. This shows that the infall in the molecular gas continues right through the ionization front and into the ionized gas.

3.3. The Nature of High Mass Star Formation

Our maps confirm the presence of simultaneous rotation and infall in the molecular gas, and ongoing work in the H66 α line has shown both infall over a large area, and outflow in a more localized jet-like structure in the ionized gas (Keto 2004). The simultaneity of these different phenomena with main sequence stars, as evidenced by the presence of the UCHII region, points to a schedule for the formation of massive stars that is compressed relative to the schedule for low mass stars. Stellar structure calculations suggest that a massive star should reach the main sequence before collapse in the molecular core has finished (Norberg & Maeder 2000; Behrend & Maeder 2001). We find in our observations evidence for this compressed evolutionary sequence. Furthermore, the presence of inward motion in the ionized gas and its apparent continuity with the molecular accretion flow suggests that the presence of an UCHII region does not necessarily end accretion as in the classical model for pressure driven expansion of HII regions. The lack of a molecular disk contrasts with the case of M17, in which a 20 M $_{\odot}$ star is accreting through a molecular disk which extends beyond a radius of 15,000 AU (Chini et al. 2004). While the two cores have similar angular velocities, roughly 10 km s $^{-1}$ pc $^{-1}$, at a radius of 0.1 pc, the much larger central mass in

G10.6 allows infall to dominate and prevent the formation of a large molecular disk.

The lack of any detectable blue-shifted absorption places a stringent upper limit on the mass of an expanding molecular shell, which would be the necessary product of pressure-driven expansion of the UCHII region. As noted in Section 1, the classical model of an over-pressured HII region expanding into a molecular medium, results in a dense, isothermally shocked, molecular layer surrounding the HII region. This layer should contain nearly all of the molecular gas originally in the volume now occupied by the HII region. We estimate that the mass of such a layer, assuming a radius for the HII region of 0.025 pc, an average molecular gas density over the volume of the UCHII region of 10^6 cm^{-3} , LTE conditions at 150 K, and an NH_3 abundance of 10^{-7} relative to H_2 (van Dishoeck & Blake 1998), would be 4 M_\odot resulting in a predicted optical depth in the main hyperfine component of $\tau \sim 2$. We detect no such layer in our line data. At the peak of the continuum, our 3σ upper limit on the optical depth of an expanding molecular layer is $\tau = 0.05$, corresponding to a shell-mass of roughly 0.1 M_\odot . We detect no outward motion; only inward motions in both the molecular and ionized gas are seen. This stringent upper limit on the mass of any expanding shell, and the fact that the molecular accretion flow which we observe at the 0.03 pc scale continues in the ionized gas, both argue against the pressure-driven expansion model and for the existence of an ionized accretion flow.

The central mass in this region can be estimated in two ways. First, we note that the infall peaks around $v_{\text{lsr}} = +3.5 \text{ km s}^{-1}$. The systemic velocity of the local gas is $v_{\text{lsr}} = -3.0 \text{ km s}^{-1}$ (Keto 1990). If the gas has a free-fall collapse speed of 6.5 km s^{-1} at a radius of 0.03 pc, the central mass must be about 150 M_\odot . We can also calculate the mass of the central star(s) by inferring the rate of Lyman continuum photon production. Because the ionized gas is infalling, we assume the density goes like $n(r) = n_0(\frac{r_0}{r})^{(3/2)}$ with $r_0 = 0.03 \text{ pc}$, and $n_0 = 10^5 \text{ cm}^{-3}$. Then, following Keto (2003), we balance ionizations with recombinations as

$$N_{\text{Ly}} = \int_{R_*}^{R_{\text{HII}}} \alpha 4\pi r^2 n^2(r) dr = 4\pi r_0^3 n_0^2 \alpha \ln\left(\frac{R_{\text{HII}}}{R_*}\right)$$

where N_{Ly} is the number of Lyman continuum photons, R_* is the radius of the star, R_{HII} is the radius of the HII region, and α is the recombination coefficient. Assuming $R_* = 10R_\odot$, $R_{\text{HII}} = 0.03 \text{ pc}$ as above, and $\alpha = 2 \times 10^{-13} \text{ cm}^3 \text{ s}^{-1}$, we get $N_i = 2.2 \times 10^{50} \text{ s}^{-1}$. This corresponds to 4 O4V stars with a total mass of 175 M_\odot , and a total luminosity of $4.4 \times 10^6 L_\odot$ (Vacca et al. 1996). This combination of stars, which matches the Lyman continuum output and, roughly, the central mass as derived from the free-fall velocity, is not unique. However, we can be certain that at least several stars must be responsible for such a large Lyman continuum emission rate.

The complicated structure of the ionized gas suggests clumpy structure in the surround-

ing molecular gas. This clumpy structure at very high density ($> 10^6 \text{ cm}^{-3}$) is consistent with the idea that this single HMC may be capable of forming many stars. The central UCHII region has formed at the center of the HMC, but must contain more than one star. The overall contraction of the core has already formed multiple stars, and may fragment further at smaller scales.

REFERENCES

- Argon, A. L., Reid, M. J., & Menten, K. M. 2000, *ApJS*, 129, 159
- Behrend, R. & Maeder, A. 2001, *A&A*, 373, 190
- Braz, M. A. & Epchtein, N. 1983, *A&AS*, 54, 167
- Casoli, F., Combes, F., Dupraz, C., Gerin, M., & Boulanger, F. 1986, *A&A*, 169, 281
- Chini, R., Hoffmeister, V., Kimeswenger, S., Nielbock, M., Nürnberger, D., Schmidtobreick, L., & Sterzik, M. 2004, *Nature*, 429, 155
- Downes, D., Wilson, T. L., Bieging, J., & Wink, J. 1980, *A&AS*, 40, 379
- Ho, P. T. P. & Haschick, A. D. 1986, *ApJ*, 304, 501
- Ho, P. T. P., Terebey, S., & Turner, J. L. 1994, *ApJ*, 423, 320
- Hofner, P. & Churchwell, E. 1996, *A&AS*, 120, 283
- Hofner, P., Wyrowski, F., Walmsley, C. M., & Churchwell, E. 2000, *ApJ*, 536, 393
- Ignace, R. & Churchwell, E. 2004, *ApJ*, 610, 351
- Keto, E. 2002a, *ApJ*, 568, 754
- Keto, E. 2004, In Preparation
- . 2002b, *ApJ*, 580, 980
- . 2003, *ApJ*, 599, 1196
- Keto, E. R. 1990, *ApJ*, 355, 190
- Keto, E. R. & Ho, P. T. P. 1989, *ApJ*, 347, 349
- Keto, E. R., Ho, P. T. P., & Haschick, A. D. 1987a, *ApJ*, 318, 712

- . 1988, *ApJ*, 324, 920
- Keto, E. R., Ho, P. T. P., & Reid, M. J. 1987b, *ApJ*, 323, L117
- Mueller, K. E., Shirley, Y. L., Evans, N. J., & Jacobson, H. R. 2002, *ApJS*, 143, 469
- Norberg, P. & Maeder, A. 2000, *A&A*, 359, 1025
- Plume, R., Jaffe, D. T., & Evans, N. J. 1992, *ApJS*, 78, 505
- Spitzer, L. 1978, *Physical processes in the interstellar medium* (New York Wiley-Interscience, 1978. 333 p.)
- Strömgren, B. 1939, *ApJ*, 89, 526
- Vacca, W. D., Garmany, C. D., & Shull, J. M. 1996, *ApJ*, 460, 914
- van Dishoeck, E. F. & Blake, G. A. 1998, *ARA&A*, 36, 317
- Walsh, A. J., Burton, M. G., Hyland, A. R., & Robinson, G. 1998, *MNRAS*, 301, 640
- Wood, D. O. S. & Churchwell, E. 1989a, *ApJ*, 340, 265
- . 1989b, *ApJS*, 69, 831

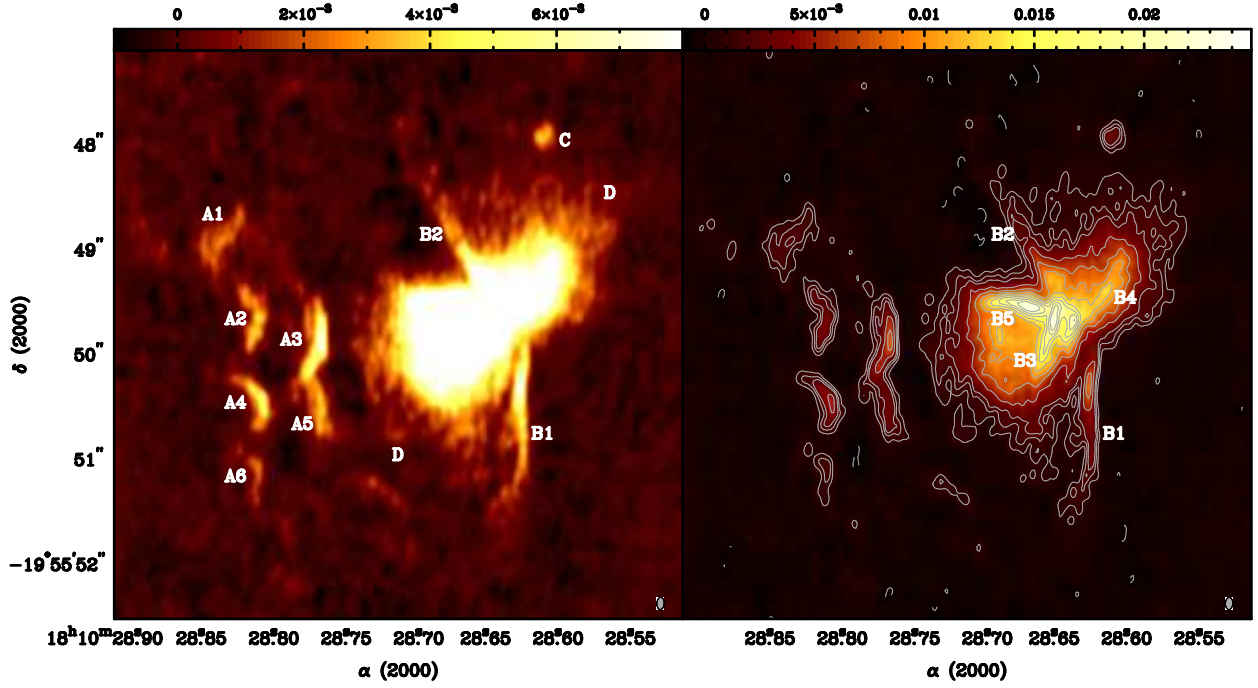


Fig. 1.— The 1.3 cm continuum map. In the left panel, the colors range linearly from -1 to 8 mJy beam $^{-1}$ although the peak in the map is 24 mJy beam $^{-1}$. This is to emphasize the weaker emission structures which are labeled A1-A6, B1-B5, C and D in the map. In the right panel, the colors range linearly from -1 to 24 mJy beam $^{-1}$, showing the entire range of emission strengths in order to emphasize structures in the stronger emission. The contours are -1, 1, 2, 3, 6, 9, 12, 15, 18, 21, 24, & 27 $\times 0.8$ mJy beam $^{-1}$. The map was made with uniform weighting and the synthesized beam ($0.''12 \times 0.''079$) is shown in the lower right of each panel.

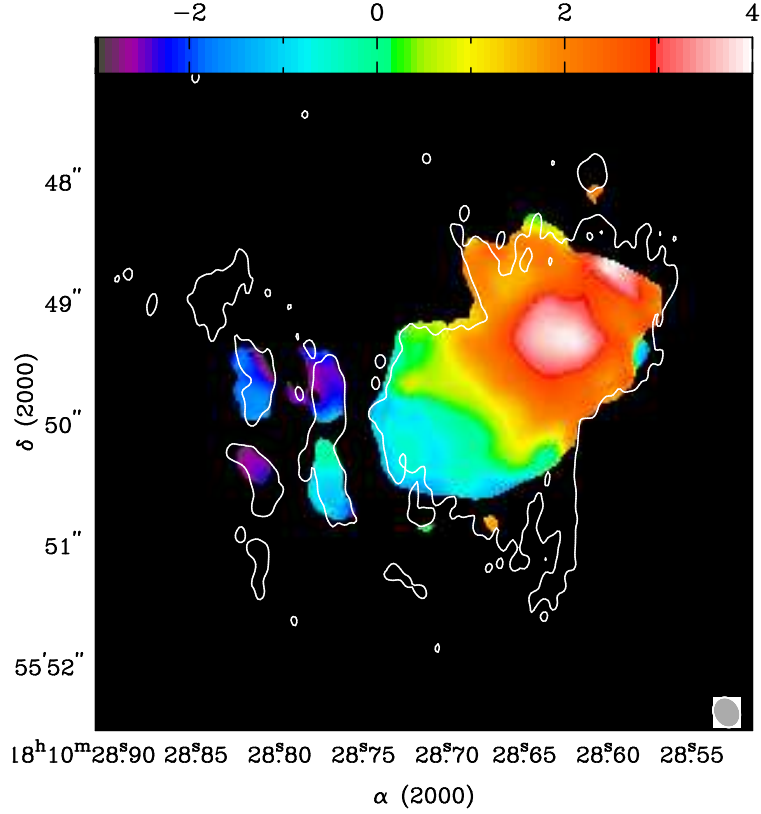


Fig. 2.— The map of the first moment of the main hyperfine component of the $\text{NH}_3(3,3)$ line. The colors range from $v_{\text{lsr}} = -3$ to $+4 \text{ km s}^{-1}$. The contour, shown for reference, is the $0.8 \text{ mJy beam}^{-1}$ contour from the 1.3 cm continuum map shown in Figure 1. The line data were mapped by the AIPS task IMAGR with natural weighting and a u-v taper at 750 kilolambda so that the resulting synthesized beam ($0.''26 \times 0.''22$) better matched the size scale of velocity pattern.